IF/P7-28

Generation of Relativistic Electron Beam and its Anomalous stopping in the Fast Ignition Scheme

S. Sengupta 1), A. S. Sandhu 2), A. K. Dharmadhikari 2), G. R. Kumar 2), A. Das 1), P. K. Kaw 1)

1) Institute for Plasma Research, Bhat, Gandhinagar 382 428, India
2) Tata Institute of Fundamental Research, 1 Homi Bhabha Road, Mumbai 400 005, India

e-mail contact of main author: sudip@ipr.res.in

Abstract. We present experimental/theoretical results concerning two main physics issues related to the fast ignition scheme *viz*. the nonlinear mechanism of conversion of incident laser energy into a relativistic electron beam at the critical layer and its subsequent transport through an overdense plasma. Theoretical/numerical modelling of the experimental data, firstly shows that the conversion of the laser energy into an inward propagating electron beam occurs through the nonlinear mechanism of wave breaking of plasma waves excited at the critical layer and, secondly the transport of the electron beam through the overdense plasma is influenced by electrostatically induced and/or turbulence induced anomalous resistivity.

1. Introduction

In the inertial confinement scheme of thermonuclear fusion (ICF), a spherically symmetric D-T capsule is ablatively imploded to ~ 10^3 times its normal density. In order to achieve energy gain a small portion of this compressed fuel (spark) must be heated to ~ 10 keV in the disassembly time scale which is approximately ~ 10 ps. In the standard scheme, the spark is both produced and heated by accurately timed shock waves. This requires perfect implosion symmetry, which implies symmetry in both target design and illumination and very large driver energy. In the fast ignition (FI) scheme of ICF, the fuel compression stage is separated from the hot spot generation stage, which strongly relaxes these stringent requirements. This scheme has already received lot of attention from various research groups, because of the experimental demonstration of its potential [1,2]. In the first stage of the FI scheme, the fuel is compressed to a density of 10^{32} m^{-3} at the core. In the second stage, an intense sub-picosecond petawatt laser pulse is incident on this overdense pre-compressed pellet. This laser energy gets converted through nonlinear mechanisms into a relativistic electron beam, which transports it through the rest of the overdense plasma and ignites a hot spot in the compressed core. There are two main underlying physics issues involved in this scenario, which however, are not very well understood. First issue, is the mechanism of conversion of laser energy into an inward propagating jet of hot electrons and second issue is its transport through the overdense plasma. Below we describe our experimental results (obtained at very modest intensities ~ 10^{20} W/m^2) whose physics may have relevance to the above mentioned issues. In section 2, we discuss the problem of hot electron current generation and in section 3, we deal with the transport of hot electrons through the overdense plasma. Finally section 4, contains a summary of our results and conclusions.

2. Mechanism of Hot Electron Current Generation

In a realistic fusion experiment, the electron density at the core is almost five orders of magnitude higher than the critical density which most modern lasers can penetrate. Therefore most of the petawatt power is absorbed at the surface. A simple estimate for a sub-picosecond laser with I ~ 10^{23} W/m^2 shows that the expansion scale length $L \gtrsim x_{osc.}$ indicating that both vacuum heating and resonance absorption mechanism may be operating. In this work, we have specifically looked at resonance absorption and its role in the production of hot electron current. Experimentally, we have studied the excitation of second harmonic radiation

simultaneously with hard X-ray emission. This is because, fundamentally the physical mechanisms responsible for all these processes are intimately related to the dynamics of electron plasma waves which are resonantly excited at the critical layer by the incident laser. In this section, we present simultaneous time resolved measurements of second harmonic and hard X-rays emitted during the interaction of an obliquely incident (45^0) p-polarized main laser pulse (10^{20} W/m^2, 100 fs, 800 nm) with a pre-plasma generated on a solid target by a normally incident pump pulse. The measurements are carried out as a function of time delay between the main pulse and the pump pulse. Subsection 2.1 contains our experimental results and in subsection 2.2, we present our analysis.

2.1 Experimental Results

This subsection contains our experimental results. Figs. (1) and (2) respectively show hard X-ray yield over 30-300 keV range and second harmonic efficiency $\eta \propto I(2\omega)/I^2(\omega)$ as a function of time delay (bottom axis in both cases). In both the plots the data are normalized with respect to yields obtained with main pulse acting alone. The jagged line is the experimental result and the continuous curve is the fit obtained using a model that is described in the next subsection. The most notable feature in these plots is the observed dip in second harmonic efficiency around ~ 24 ps, which is nearly the same point where hard X-ray emission maximizes.

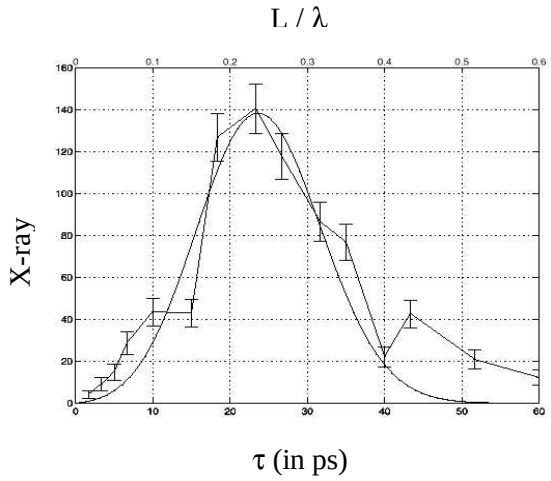

FIG. 1. X-ray Yield Vs time

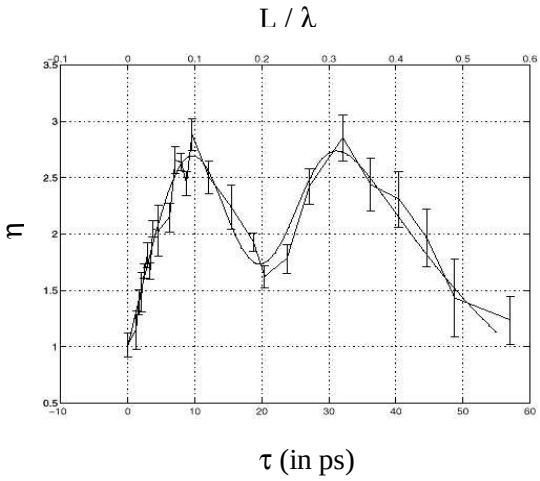

FIG. 2. Second Harmonic efficiency Vs time

Around ~ 24 ps, second harmonic efficiency dips to half of its maximum value, whereas hard X-ray yield is enhanced by two orders of magnitude as compared to its baseline value, indicating a large amount of hot electron generation. To establish that there is indeed copious generation of hot electron current around ~ 24 ps, we present spectrally resolved hard X-ray yield and compare the hot electron temperatures with and without time delay of ~ 24 ps.

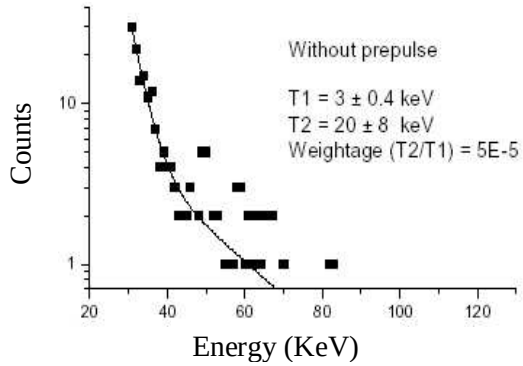

FIG. 3(a) Hot Electron Temperature fit without prepulse

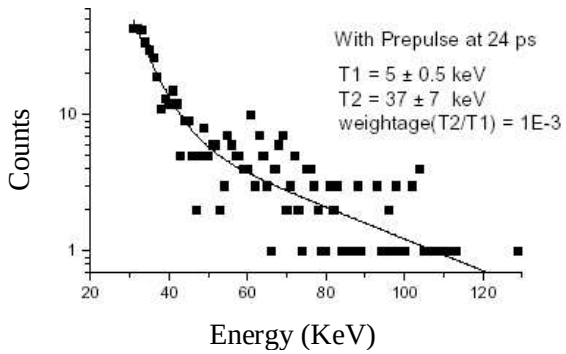

FIG. 3(b) Hot Electron Temperature fit with prepulse

Fig. 3(a) corresponds to the case when main pulse is acting alone and fig. 3(b) corresponds to the case when prepulse to main pulse delay is ~ 24 ps. Comparison of the hot electron spectra clearly shows a significant high temperature component (as seen from statistical weights) in the second case, indicating a burst in hot electron current generation. About second harmonic emission, we note that it was observed to be specular in our experiments. This indicates that it is generated by electron plasma waves produced by a linear conversion mechanism like resonance absorption [3,4]. In fig. (4), we present the reflectivity of the main pulse as a function of time delay. As expected, with the increase in scale length, resonance absorption increases, reaches a maximum around ~24 ps (around the same point where second harmonic emission dips and hard X-ray yield peaks), and decreases for larger values of time delay. Thus our experimental results point towards the fact that, at the peak of resonance absorption, large amplitude electrostatic waves are excited which undergo nonlinear damping via wave breaking mechanism thus producing large amount of hot electrons, resulting in a peak in X-ray emission and a dip in second harmonic generation.

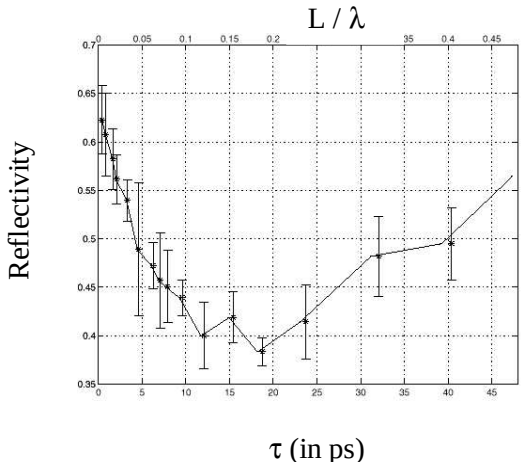

FIG. 4. Reflectivity of the pump pulse Vs time delay

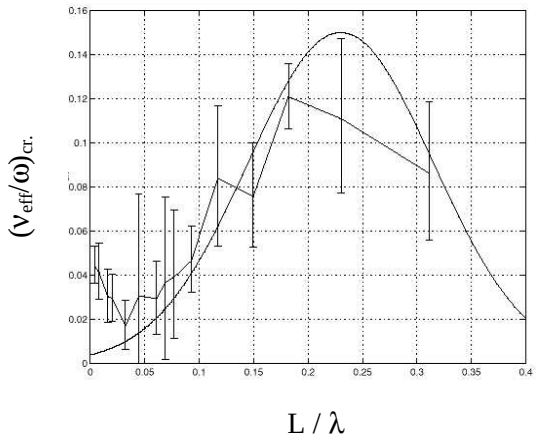

FIG. 5. $(\nu_{eff}/\omega)_{cr.}$ Vs L/λ

2.2 Modelling Of Second Harmonic and Hard X-rays

We now present an analysis of our experimental results, which proves beyond doubt, the fundamental role played by resonance absorption and wave breaking in the physical mechanism of hot electron current generation. Our analysis is based on models for X-ray yield and second harmonic efficiency. We model the X-ray yield as a quantity Y which is taken to be proportional to the intensity of absorbed light $I_{abs} \approx \int_0^\infty \frac{\nu_{eff} E_z^2}{8\pi} dz$, where ν_{eff} is the effective collision frequency due to linear/nonlinear processes and E_z is the electric field associated with the plasma wave. It is well known, that for $\nu_{eff}/\omega \rightarrow 0$ (linear processes), I_{abs} is independent of ν_{eff}/ω *i.e.* the intensity of absorbed light is independent of the process of absorption [5]. In general, however, for nonlinear processes, ν_{eff}/ω itself becomes a function of E_z (and vice-versa), with the result that I_{abs} becomes dependent on the process of absorption. Keeping in view the fact that most of the absorption occurs near the critical layer, we now approximate the absorption integral as $I_{abs} \approx (L / \lambda)_{cr.} (\nu_{eff} E_z^2 / 8 \pi)_{cr.}$ where the subscript "cr." denotes values corresponding to the critical layer. Since E_z itself is a function of $(\nu_{eff}/\omega)_{cr.}$ through the local dielectric constant, we can therefore model the X-ray yield Y as $Y = A (L / \lambda)_{cr.} f [(\nu_{eff}/\omega)_{cr}]$ where A is some proportionality constant and f is some unknown function of $(\nu_{eff}/\omega)_{cr}$. For second harmonic efficiency η, we use the model developed by Erokhin et. al. [6], which gives the scaling of second harmonic efficiency η with $(L/\lambda)_{cr.}$ and

$(\nu_{eff}/\omega)_{cr}$ as $\eta \propto \rho^2 \exp [- (b + d (\nu_{eff}/\omega)_{cr}.) \rho]$ where $\rho = 2 \pi (L/\lambda)_{cr}$ and "b" & "d" are two constants of order unity. Thus X-ray yield and second harmonic efficiency η are both functions of scale length $(L/\lambda)_{cr}$ and effective collision frequency $(\nu_{eff}/\omega)_{cr}$. We now evaluate these parameters from the reflectivity curve of the main pulse (fig. (4)). Using the condition for maximum resonance absorption as $(2 \pi (L/\lambda)_{cr})^{1/3} \sin \theta \sim 0.8$, we make an estimate of $(L/\lambda)_{cr} \approx 0.23$. This value of $(L/\lambda)_{cr}$ corresponds to the time delay when resonance absorption maximizes ~24 ps. This in turn, gives an estimate of the expansion velocity $v_{exp} \sim 7.7 \times 10^3$ m/sec, which is very reasonable for intensities of the order $\sim 2 \times 10^{18}$ W/m^2 (intensity of the prepulse which creates the plasma). Using this expansion velocity, the whole time delay axis is calibrated with corresponding scale length values at the critical layer $(L/\lambda)_{cr}$ (see top axis of fig. (1), fig. (2) and fig. (4)). We thus have experimentally measured reflectivity as a function of scale length at the critical layer $(L/\lambda)_{cr}$, which we now utilize to evaluate $(\nu_{eff}/\omega)_{cr}$ for each value of reflectivity. This is achieved by numerically solving the wave equation for magnetic field of a p-polarized light propagating through an inhomogeneous plasma slab [7]**.** Choosing a linear density profile and taking ν/ω as proportional to density, we numerically evaluate the reflectivity of the main pulse for each value of $(L/\lambda)_{cr}$ treating $(\nu_{eff}/\omega)_{cr}$ as a parameter. Matching the calculated value of reflectivity with the observed value gives $(\nu_{eff}/\omega)_{cr}$ as a function of $(L/\lambda)_{cr}$,as shown in fig. (5). The error bars in this figure correspond to the error bars in the reflectivity curve. The high value of $(\nu_{eff}/\omega)_{cr} \sim 0.16$ (this is an order of magnitude higher than $(\nu_{eff}/\omega)_{cr}$ for $T_e \approx 100$ eV, which is typically the bulk temperature at our intensities) at the peak, corresponding to the maxima of resonance absorption is a clear indication of damping of the excited electrostatic waves at the critical layer by nonlinear processes like wave breaking [3]. These values of $(\nu_{eff}/\omega)_{cr}$ are now used to fit the X-ray yield and second harmonic efficiency η according to the models described earlier. To do this, we first represent the gross behaviour of $(\nu_{eff}/\omega)_{cr}$ as a function of $(L/\lambda)_{cr}$ obtained numerically with a smooth function of the form $(\nu_{eff}/\omega)_{cr} = a \exp[-((L/\lambda)_{cr} - c)^2 /\omega^2]$ with $a \sim 0.16$, $c \sim 0.2$ & $w \sim 0.1$ (see the solid line in fig. (5)). We use this gaussian form in the models for hard X-ray yield Y and the second harmonic efficiency η. The excellent fits obtained for both Y and η (see the solid lines in figs. (1) and (2)), clearly shows that our experimental results are in good agreement with the theory of resonance absorption and wave breaking. We therefore believe that in the fast ignition scheme the hot electrons are generated at the critical surface of the target by wave breaking of large amplitude electrostatic waves, which are excited by the incident petawatt laser.

3. Hot Electron Transport

The second physics issue, with which we have dealt in this paper, is the transport of hot electrons through the overdense plasma. The hot electron current generated at the critical layer by the incident laser excites a cold return shielding current. The combination of this hot and cold current generates strong quasi-static magnetic fields, which lead to filamentation of the electron flow. Depending on the resistivity of the background plasma, the propagation of these current filaments is further hindered, either via electrostatically induced or turbulence induced mechanisms. In the high resistivity case, the magnitude of cold return current is low, leading to the generation of large electrostatic fields. These electrostatic fields in turn exert a retarding force on the hot electrons resulting in anomalous stopping. On the other hand if the resistivity of the background plasma is low, large return shielding currents are excited. The resulting hot and cold electron current channel is unstable to EMHD modes (sausage/kink) leading to the generation of turbulent magnetic fields, which randomizes the electron motion. This results in anomalous stopping in this case. In the case of fast ignition, both these mechanisms may play

a role. To gain further insight into these mechanisms, we have experimentally measured the magnetic field generated by the hot and cold return currents in two extreme cases *viz.* solid aluminum (conducting material with low classical resistivity) and BK7 glass (dielectric material with high classical resistivity). In Subsection 3.1, we describe our experimental measurements. Subsection 3.2 contains our analysis of the experimental results.

3.1 Experimental Results

Using pump probe polarimetry, we have measured the temporal evolution of magnetic fields generated by the interaction of an obliquely incident (45^0) p-polarized pump laser (10^{20} W/m^2, 100fs, 800nm) with the above mentioned targets. The probe laser which is focussed at near normal incidence is frequency doubled, and is made ~ 10^3 times weaker than the pump intensity. In this configuration, it penetrates beyond the critical density for the pump laser, and thus samples the high-density region where high magnetic fields are expected to exist. The BK7 glass target was coated with about half a μ thick aluminum on the front surface so that laser hitting the target generates identical hot electron temperatures in both cases. To establish that this is indeed so, we have measured the hard X-rays arising from hot electrons in the 50 to 500 keV range for both the cases, under similar laser conditions. The hot electron spectra are shown in fig. 6(a) and 6(b). The hot electron temperature obtained from the fit (shown as solid line) is observed to be approximately same (~ 30 keV) in both the cases indicating identical hot electron sources.

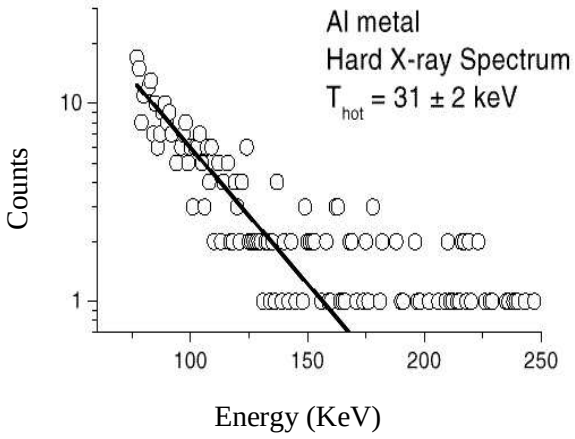

FIG. 6(a) Hot Electron Temperature fit for Aluminum

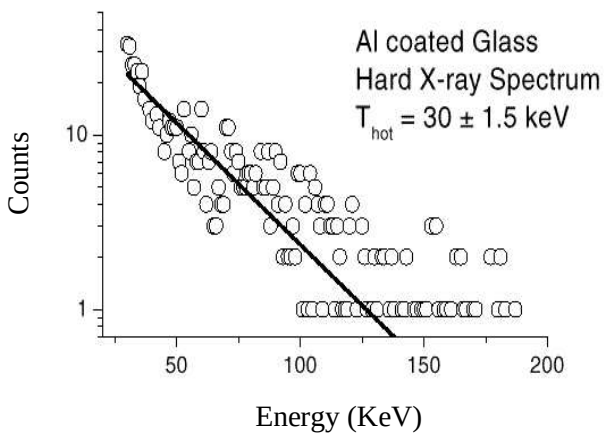

FIG. 6(b) Hot Electron Temperature fit for Aluminum coated BK7 glass

In our experiment we have actually measured the ellipticity induced in the probe pulse by the pump generated magnetic field. This measurement is carried out as a function of the time delay between the pump and the probe pulse. The measured ellipticity is transformed into magnetic field data by numerically studying the propagation of an electromagnetic wave through a inhomogeneous plasma, with the wave vector perpendicular to the magnetic field direction. In our numerical analysis, we have chosen an exponential density profile which expands at the sound speed corresponding to T_e=100 eV and Z=5 [8]. However, we have observed that our results are reasonably insensitive to the chosen density profile. The plots of magnetic field for solid aluminum target and BK7 glass coated with aluminum layer as a function of time delay are shown in fig. 7(a) and fig. 7(b) respectively.

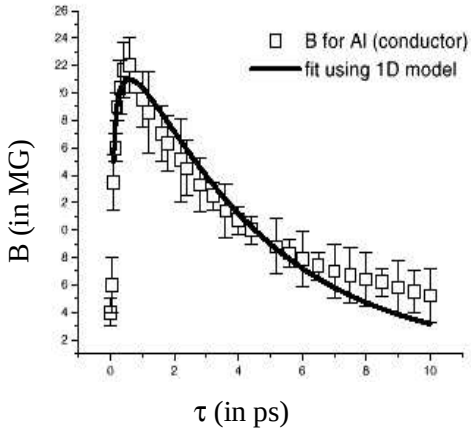

FIG. 7(a) Magnetic Field Vs time delay for Aluminum

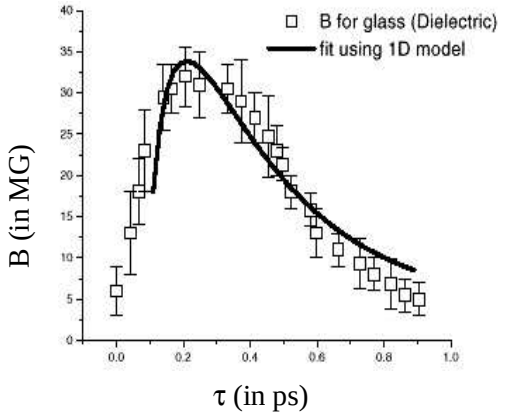

FIG. 7(b) Magnetic Field Vs time delay for Glass

The squares represent experimental points and the solid curves, which show a reasonable fit are obtained using a one-dimensional model developed below. We observe that, in both cases, the measured magnetic field initially shows a rise, goes to a maximum and decays exponentially. The point to note here is that the time scale of decay in glass is an order of magnitude smaller than in aluminum indicating different mechanisms of anomalous stopping in dielectric (glass) and conductor (aluminum). Decay time in each case is related to the electrical resistivity (either electrostatically or turbulence induced) of the background plasma. Since our interest lies in anomalous stopping of the hot electron current after it is generated by the incident laser, we have modelled the experimental data beyond the time $t > \tau_{laser}$ using a formalism given by Bell et. al. [9].

3.2 Modelling of Magnetic Field

The temporal evolution of magnetic field is modelled using the following equation, which describes the mechanism of quasistatic magnetic field generation under EMHD approximation

$$\frac{\partial \vec{B}}{\partial t} = \frac{c^2}{4\pi\sigma}\nabla^2 \vec{B} + \frac{c}{\sigma}\left(\vec{\nabla} \times \vec{j}_{hot}\right) \qquad (1)$$

The first term here describes the magnetic field decay due to resistive damping of the plasma shielding currents (σ being the conductivity of the background plasma) and the second term describes the magnetic field generation due to hot electron currents. Assuming the magnetic field to be in the azimuthal direction, the above equation is approximated as

$$\frac{\partial B}{\partial t} \approx -\frac{B}{\tau} + S(z,t) \qquad (2)$$

where the diffusion term is taken as B/τ with $\tau \approx (4\pi\sigma/c^2)(\Delta r)^2$, and the source term is approximated as $S(z,t) \approx -(c/\sigma(\Delta r))j_{hot}(z,t)$. Here Δr is the laser spot radius, which is about 10 μ. Taking $B = B_{las}$ at $t = \tau_{laser}$, the solution is given by

$$B \approx B_{las} e^{-(t-\tau_{laser}/\tau)} - e^{-(t/\tau)} \int_{\tau_{laser}}^{t} \frac{c}{\sigma \Delta r} j_{hot}(z,t) e^{t/\tau} dt \qquad (3)$$

where $j_{hot} = -en_h v_h$, n_h is the hot electron density and v_h is the velocity of the hot electron fluid. To make an estimate of n_h and v_h, we use the formalism given by Bell et al. [9]. According to Bell, the evolution of hot electron density n_h is governed by a nonlinear diffusion equation of the form

$$\frac{\partial n_h}{\partial t} = \frac{\partial}{\partial z}\left(\frac{\sigma T_h}{e^2 n_h} \frac{\partial n_h}{\partial z} \right) \qquad (4)$$

whose solution in the regime $t > \tau_{laser}$ is written as

$$n_h = \frac{2 n_0 z_0}{\pi} \frac{L}{z^2 + L^2} \qquad (5)$$

with $L(t) = z_0 \left[\frac{5\pi\sigma T_h}{3e^2 n_0 z_0^2} (t - \tau_{laser}) + 1 \right]^{3/5}$, $n_0 = \frac{2}{9} \frac{I_{abs}^2 \tau_{laser} e^2}{\sigma T_h^3}$ and $z_0 = \frac{3\sigma T_h^2}{e^2 I_{abs}}$. Here T_h is the hot electron temperature and the absorbed intensity $I_{abs} = f\, I_{incident}$, f being the fraction absorbed. n_0 is the density of hot electrons at z = 0 at time $t = \tau_{laser}$ and z_0 is the characteristic stopping length such that $n_0 z_0$ is the total number of hot electrons produced at time $t = \tau_{laser}$. The solution of the nonlinear diffusion equation is a self-similar solution in which the spatial shape remains the same but it expands in time with a scale length L(t). Using the expressions for n_h and L(t) we estimate j_{hot} as $j_{hot} = -e \frac{2 n_0 z_0}{\pi} \frac{L}{z^2 + L^2} \left[\alpha \frac{dL}{dt} \right]$ where v_h, the hot electron velocity is taken to be proportional to dL/dt, α being the proportionality constant. Substituting the expression for dL/dt in j_{hot} and using it in equation (3) along with $\sigma \approx c^2/(4\pi(\Delta r)^2)\tau$, we get

$$B = B_{las} e^{-y} + A e^{-y} \tau \int_0^y \frac{(py\tau + 1)^{1/5} e^y}{z^2 + z_0^2 (py\tau + 1)^{6/5}} dy \qquad (6)$$

where $y = (t - \tau_{laser})/\tau$, $A = (2cz_0\alpha T_h)/(e\Delta r)$ and $p = (5\pi\sigma T_h)/(3e^2 n_0 z_0^2)$. We now use the above expression for B(t,z) at z = 0 to model the magnetic field evolution as a function of time, for both BK7 glass coated with aluminum and solid aluminum using τ (which is related to conductivity σ) and f (fraction of light absorbed) as free parameters. z = 0 is the point where hot electrons are generated; so it is actually the critical density point. The proportionality constant α is taken to be unity. B_{las}, the magnetic field at time $t = \tau_{laser}$ is 15 MG and 18 MG respectively for aluminum and glass. The best-fit curves (solid lines) are shown in fig. 7(a) and fig. 7(b) respectively. From the best fit, the relevant parameters (f and τ) for aluminum and glass are respectively f = 0.48, τ = 3.5 ps and f = 0.21, τ = 0.2 ps. From the results of the fit, it is clear that the time for magnetic field decay in aluminum is an order of magnitude larger than in glass. Calculation of resistivity using $\eta = (4\pi(\Delta r)^2)/(c^2\tau)$, gives $\eta_{Al} = 3.6 \times 10^{-5}$ Ω-m and $\eta_{glass} = 6.3 \times 10^{-4}$ Ω-m. We see that resistivity of aluminum as deduced from these measurements is an order of magnitude higher than the value of resistivity deduced from reflectivity measurements by Milchberg et. al. [8]. In case of glass our

measurements show that neutralization of hot electron current is clearly not as effective as it is in aluminum. This is due to high background resistivity, which results in inhibition of hot electron propagation in glass through generation large of electrostatic fields. Thus our modelling of the experimental data clearly indicates that anomalous stopping in glass occurs because of electrostatic inhibition, which is due to absence of return shielding currents, whereas in aluminum, it occurs because of turbulence induced anomalous resistivity. The concept of turbulent resistivity is of considerable significance to the fast ignition scheme of laser fusion, as can be seen from the following argument. As stated in the introduction, to ignite the spark the core has to be heated to a temperature of 10 keV within 10 ps. Considering only ohmic heating which is due to cold return currents [10] and using a hot electron density of ~ 10^{27} m^{-3} (this is the critical density for 1 μ wavelength laser), it can be shown that the resistivity needed to satisfy the ignition criterion is approximately three orders of magnitude higher than the Spitzer resistivity at 10 keV [11]. There already exists an indirect evidence of such anomalously high resistivity in real fusion scale experiments [11].

4. Summary and Conclusions

In this work, we have studied two physics issues which have relevance for the fast ignition scheme *viz.* generation of hot electrons through nonlinear mechanisms and turbulent transport of hot electron current through an overdense plasma. Our studies have shown, that if resonance absorption dominates the physics of hot electron generation then, they could be created at the critical layer by wave breaking of the plasma waves which are resonantly excited by the incident laser. Further the propagation of these hot electrons through the overdense plasma is strongly affected by the background cold plasma resistivity.

References

[1] KODAMA, R., et al., "Fast heating of ultrahigh-density plasma as a step towards laser fusion ignition", Nature **412** (2001) 798.
[2] KODAMA, R., et al., "Fast heating scalable to laser fusion ignition", Nature **418** (2002) 933.
[3] VON DER LINDE, D., et al., "Second harmonic generation in plasmas produced by intense femtosecond laser pulses", IEEE Jnl. Quan. Elec. **28,** 2388 (1992).
[4] GIZZI, L. A. et al., "Simultaneous measurements of hard X rays and second-harmonic emission in fs laser-target interactions",Phys. Rev. Lett. **76**, 2278 (1996).
[5] KRUER, W. L., "The physics of laser-plasma interactions", Addison-Wesley, New York (1988).
[6] EROKHIN, N. S. et al., "Second harmonic generation by an electromagnetic wave incident on inhomogeneous plasma", Sov. Phys. JETP **29**, 101 (1969).
[7] MILCHBERG, H. M. et al., "Light absorption in ultrashort scale length plasmas", J. Opt. Soc. Am. B **6**, 1351 (1989).
[8] MILCHBERG, H. M. et al., "Resistivity of a simple metal from room temperature to 10^6 K", Phys. Rev. Lett. **61**, 2364 (1988).
[9] BELL, A. R. et al., "Fast-electron transport in high-intensity short-pulse laser-solid experiments", Plasma Phys. Cont. Fus. **39**, 653 (1997).
[10] DAVIES, J. R., "Electric and magnetic field generation and target heating by laser-generated fast electrons", Phys. Rev. E **68**, 056404 (2003).
[11] SANDHU, A. S. et al., "Real time monitoring of the fast electron transport inside dense plasmas", Manuscript in preparation.